

Initial Mass Functions of Young Stellar Clusters from the Gemini Spectroscopic Survey of Nearby Galaxies I. Young Massive Clusters in the Antennae galaxies

JAE-RIM KOO ¹, HYUN-JEONG KIM ^{1,2} AND BEOMDU LIM ^{1,2,3}

¹*Earth Environment Research Center, Kongju National University, 56 Gongjudaehak-ro, Gongju-si, Chungcheongnam-do 32588, Republic of Korea*

²*Korea Astronomy and Space Science Institute, 776 Daedeok-daero, Yuseong-gu, Daejeon 34055, Republic of Korea*

³*Department of Earth Science Education, Kongju National University, 56 Gongjudaehak-ro, Gongju-si, Chungcheongnam-do 32588, Republic of Korea*

Submitted to AJ

ABSTRACT

The stellar initial mass function (IMF) is a key parameter to understand the star formation process and the integrated properties of stellar populations in remote galaxies. We present a spectroscopic study of young massive clusters (YMCs) in the starburst galaxies NGC 4038/39. The integrated spectra of seven YMCs obtained with GMOS-S attached to the 8.2-m Gemini South telescope reveal the spectral features associated with stellar ages and the underlying IMFs. We constrain the ages of the YMCs using the absorption lines and strong emission bands from Wolf-Rayet stars. The internal reddening is also estimated from the strength of the Na I D absorption lines. Based on these constraints, the observed spectra are matched with the synthetic spectra generated from a simple stellar population model. Several parameters of the clusters including age, reddening, cluster mass, and the underlying IMF are derived from the spectral matching. The ages of the YMCs range from 2.5 to 6.5 Myr, and these clusters contain stellar masses ranging from $1.6 \times 10^5 M_{\odot}$ to $7.9 \times 10^7 M_{\odot}$. The underlying IMFs appear to differ from the universal form of the Salpeter/Kroupa IMF. Interestingly, massive clusters tend to have the bottom-heavy IMFs, although the masses of some clusters are overestimated due to the crowding effect. Based on this, our results suggest that the universal form of the IMF is not always valid when analyzing integrated light from unresolved stellar systems. However, further study with a larger sample size is required to reach a definite conclusion.

Keywords: Star forming regions(1565) – Starburst galaxies(1570) – Stellar mass functions(1612) – Young massive clusters(2049)

1. INTRODUCTION

Stellar systems serve as laboratories to study the star formation process, because approximately 80–90 % stars form in stellar clusters or associations (Lada & Lada 2003; Porras et al. 2003) in the Galaxy. In particular, young massive clusters (YMCs) are the nests of massive stars that are very rare in the Solar neighborhood. The conditions of massive star formation can be studied statistically using the initial mass function (IMF) sampled

from a wide range of stellar masses (Lim et al. 2017). In addition, stellar systems generally form along the spiral arms of host galaxies and are dissolved into galactic disks (Bica et al. 2001; Lada & Lada 2003; Gouliermis 2018). Therefore, they play a crucial role in determining the properties of stellar population in their host galaxies.

A large number of observational studies have been performed on stellar clusters in the Galaxy, because the individual members can be spatially resolved due to their proximity. However, the severely uneven distribution of the interstellar medium across the Galactic disk introduces observational bias in the cluster sample. Several YMCs in the inner Galaxy have been steadily studied in the infrared domain (Figer et al. 1999, 2006; Davies et

al. 2007; Brandner et al. 2008; Clark et al. 2009; Lim et al. 2013; Hosek et al. 2019, etc.), but most cluster samples are limited to within 3 kpc from the Sun (Cantat-Gaudin et al. 2018; Dias et al. 2021). This observational bias limits our ability to study star formation in different environments.

Stellar clusters in nearby galaxies can provide constraints on the formation process of stars and clusters when combined with the Galactic sample. Such stellar systems are generally found in molecular gas disks (Trancho et al. 2007; Hwang & Lee 2008; Bastian et al. 2009; Whitmore et al. 2010; Lim et al. 2013). Interestingly, a large number of massive clusters tend to be located in extreme environments of interacting galaxies. For instance, de Grijs et al. (2003) discovered high-mass clusters in the ring of NGC 3310 and the tidal tail of NGC 6745. Trancho et al. (2007) performed spectroscopic observations of three clusters found in the tidal tail of NGC 3256, which revealed the masses as high as $\sim 10^5 M_{\odot}$ for these clusters. Bastian et al. (2005) discovered many YMCs in the tidal tails of NGC 6872. These observational results suggest that such extreme environments are likely the preferential sites of massive cluster formation.

NGC 4038 and 4039 (NGC 4038/9), the so-called Antennae galaxies, are interacting galaxies that provide an excellent testbed for studying the star formation process in extreme environments subject to external forces. These galaxies contain a large amount of molecular gas ($\sim 10^8 - 10^{10} M_{\odot}$; Stanford et al. 1990; Gao et al. 2001; Wilson et al. 2003; Zhu et al. 2003; Schulz et al. 2007). A large fraction of H I gas ($\sim 70\%$) is distributed in the tidal tails (van der Hulst 1979; Hibbard et al. 2001). The gas kinematics of these galaxies were investigated in several studies (Burbidge & Burbidge 1966; Amram et al. 1992; Hibbard et al. 2001; Schulz et al. 2007). Neff & Ulvestad (2000) detected a number of radio sources. About 30% of the strongest radio sources are likely associated with active star-forming regions. Later, radio observations with the Atacama Large Millimeter/submillimeter Array newly identified some molecular structures and compact sources (Espada et al. 2012; Whitmore et al. 2014).

A deep Chandra X-ray image revealed hot diffuse gas across NGC 4038/9, showing various levels of chemical enrichment (Fabbiano et al. 2003, 2004). A fraction of hot gas appears to be heated by feedback from massive stars in stellar clusters (Metz et al. 2004). Zezas et al. (2006) detected several tens of X-ray sources from an extensive monitoring survey, finding a flat X-ray luminosity function in their later study (Zezas et al. 2007).

Thus, most results from previous studies confirm that star formation is actively taking place in NGC 4038/9.

Whitmore & Schweizer (1995) discovered more than 700 cluster candidates from Hubble Space Telescope (HST) observations, the brightest of which were considered young globular clusters. They also studied the clusters in NGC 4038/9 using higher resolution images taken with the Advanced Camera for Surveys and Near Infrared Camera and Multi-Object Spectrometer on board the HST (Whitmore et al. 2010). Their infrared images revealed that approximately 16% of the clusters are still embedded in their natal clouds. The spatial age distributions of the stellar clusters show signs of triggered cluster formation by older clusters. Bastian et al. (2009) performed multi-object spectroscopy of 16 stellar clusters in the same galaxies with supplemental HST imaging in the optical domain. They postulated that most clusters formed after the merger given the range of their ages (3 – 200 Myr).

NGC 4038/9 are among the closest pairs of interacting galaxies, but not close enough to resolve the stellar clusters into individual members. The published distance to these galaxies ranges from 20.0 Mpc to 28.8 Mpc (Whitmore & Schweizer 1995; Schweizer et al. 2008) depending on the adopted Hubble constant. Therefore, previous photometric and spectroscopic studies on stellar clusters investigated their physical properties based on the integrated light. In order to interpret the integrated light, it is essential to assume the IMF, because there is a degeneracy among underlying physical parameters.

Several studies have shown that stellar IMFs, in general, do not deviate significantly from the Salpeter/Kroupa IMFs (Bastian et al. 2010), but there are signs of IMF variations (Lim et al. 2017; Smith 2020; Boylan-Kolchin 2023; Cameron et al. 2024, and references therein). We initiated a systematic survey of stellar clusters in nearby galaxies to test the universality of stellar IMFs. NGC 4038/9 are the first targets from which we infer the underlying IMFs from the integrated spectra of YMCs formed in starburst environments within the interacting galaxies. The data used are described in Section 2. We present the results of this study in Section 3 and discuss several sources that may have influenced our analysis in Section 4. Finally, our results are summarized in Section 5.

2. DATA

We took the catalogs of 50 luminous clusters and 50 massive clusters from Whitmore et al. (2010). These two catalogs were merged into a single catalog after removing duplicates. A total of 29 clusters younger than 10 Myr and brighter than 21.5 mag in the V band were selected

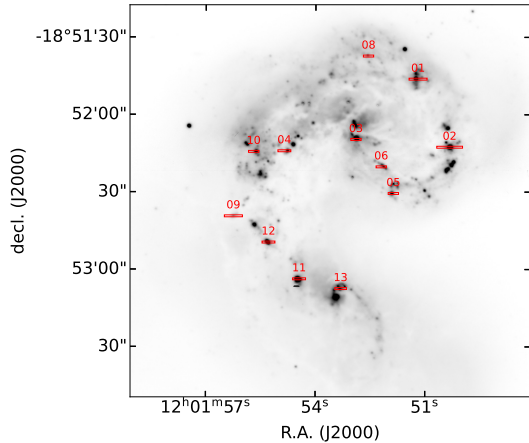


Figure 1. GMOS-S g' band image of NGC 4038/9. The slit positions are shown by rectangular boxes with the cluster IDs.

as candidates for spectroscopic observations. Indeed, these candidates have blue $U - B$ colors because they contain hot massive stars. Their total stellar masses range from $2 \times 10^4 M_{\odot}$ to $1.6 \times 10^6 M_{\odot}$ (Whitmore et al. 2010).

2.1. GMOS observation

We performed pre-imaging observations in the g' band and spectroscopic observations with the Gemini Multi-Object Spectrograph (GMOS) at the Gemini South observatory (GS-2022A-Q-122 and GS-2023A-Q-123). The observed images were used to design a mask for multi-object spectroscopy. We obtained the spectra of 12 YMCs out of 29 candidates to avoid overlapping spectra dispersed from adjacent slits in the mask. Figure 1 displays the positions of the observed YMCs on the GMOS pre-image.

The B600 grating was used to cover a spectral range from 3500 Å to 6250 Å, and the slit width was set to $0''.75$. In order to remove cosmic rays and to fill the two gaps of the GMOS detectors, we performed wavelength dithering by shifting the central wavelengths to 4200 Å, 4500 Å, and 4800 Å. A total of 35 GMOS frames were acquired over six nights from 2022 June 8 to 2023 February 16. The exposure time of each frame was 900 seconds. We note that the eight frames observed on 2022 June 8 were excluded from our analysis because the angular distance to the moon was closer than 30° (bright background) and the poor seeing condition.

For flux calibration, the spectra of the standard star LTT 4816 were obtained using GMOS in a long-slit mode. The observations of the standard star were conducted on the same night as the target observing run on 2023 February 13, with the same settings for the central wavelengths and slit-width.

All spectroscopic data were reduced using the Gemini IRAF package following the standard procedures. The solution for wavelength calibration was obtained from the arc spectra and applied to the spectra of the standard star and YMCs. The wavelength-corrected two-dimensional spectra were combined into a single spectrum for the same target observed on the same night. We extracted one-dimensional (1D) spectra using custom python scripts.

In the slits, the observed YMCs have finite extents that are larger than the mean seeing of about $0''.7$. We fit a Gaussian profile to a spatial profile along the spatial axis of the slit at given wavelengths. Then, spectra were extracted within an aperture radius corresponding to 3σ of the best-fit Gaussian profile. The median values of the signals from the outer part of each slit were considered as background signals. We subtracted these background signals from the extracted 1D spectra of the YMCs.

The spatial profile of ID 13 is blended by the neighboring objects in the same slit. The slit length does not cover the full extent of the four YMCs (IDs 04, 05, 06, and 10) with a sufficiently wide sky background. Therefore, a total of five YMCs were excluded for further analysis. In this study, we analyzed the integrated spectra of seven YMCs. However, some spectra of the seven YMCs were additionally discarded because the slit length is still short compared to the observed spatial profile affected by the seeing variations among observing runs.

A small portion of the signals from the observed YMCs were lost due to the slit width being comparable to the diameter of the seeing disk. In addition, atmospheric differential refraction occurs depending on the position angles of the slits on the sky. We corrected for these effects on the observed spectra using the `spec.lightloss2` function of Ian's Astro-Python Code¹.

Recent quantum efficiency curves for the GMOS detector² were used to correct for the quantum efficiency that varies over a wide range of wavelengths. For extinction correction, we applied the mean atmospheric extinction at the Gemini South observatory (ctioextinction; Stone & Baldwin 1983). The heliocentric radial velocity correction was also performed to combine the spectra observed on different nights.

We used the spectra of the YMCs observed on the same night with the observations of the standard star LTT 4816 as a reference. The spectra taken on differ-

¹ <https://crossfield.ku.edu/python/>

² The quantum efficiency curves of the GMOS detector adopted from Data Reduction for Astronomy from Gemini Observatory North and South (DRAGONS).

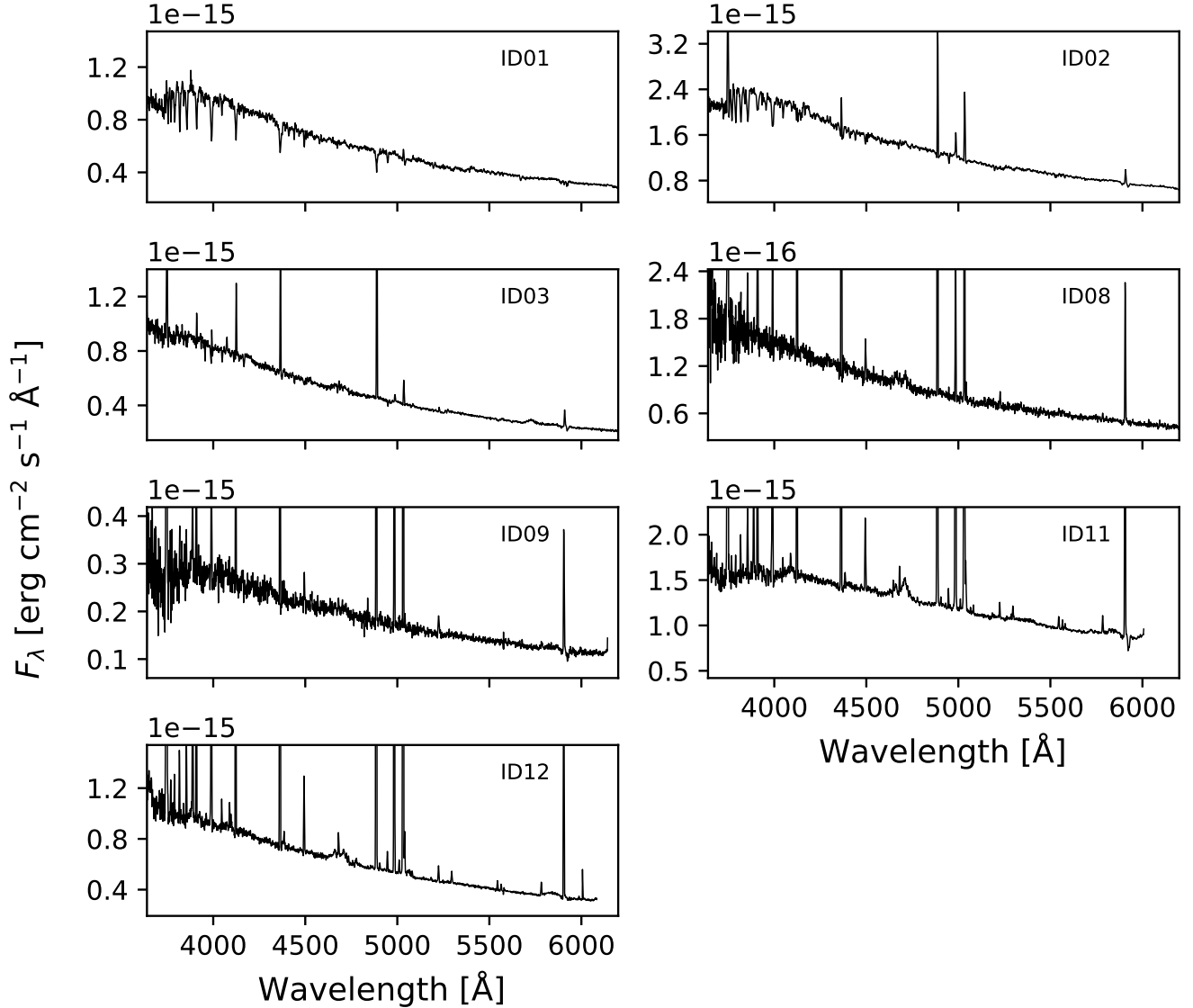


Figure 2. Observed spectra of seven YMCs. The cluster ID is labeled in the upper right corner of each panel. The fluxes of the observed spectra were calibrated using the spectra of the standard star LTT 4816.

ent nights were scaled to the flux levels of the reference spectra and then combined into a single spectrum for individual cluster by adopting the median at given wavelengths. The final signal-to-noise ratios (SNRs) of the combined spectra range from 25 to 90 at around 5400 Å. Figure 2 displays the flux-calibrated spectra of the seven YMCs.

To test the quality of our flux calibration, we conducted synthetic photometry for the flux-calibrated spectra of the standard star LTT 4816 and the four YMCs (IDs 01, 02, 03 and 08) that are spatially well-isolated from bright sources using the Pyphot package (Fouesneau 2022). The photometric zeropoint of -0.2 mag in the V band was obtained by calculating the

difference between the magnitudes from the SIMBAD database (Wenger et al. 2000) and our synthetic photometry for the standard star. This zeropoint was then applied to the V magnitudes of the four YMCs. We compared our photometric data with those of Whitmore et al. (2010). The mean difference between the two photometric data is less than 0.01 mag, and the standard deviation is about 0.32 mag. Therefore, we confirmed that the spectra of the YMCs are well calibrated in an absolute scale.

2.2. Simple stellar population model

It is essential to select a simple stellar population model to interpret the integrated light from unresolved

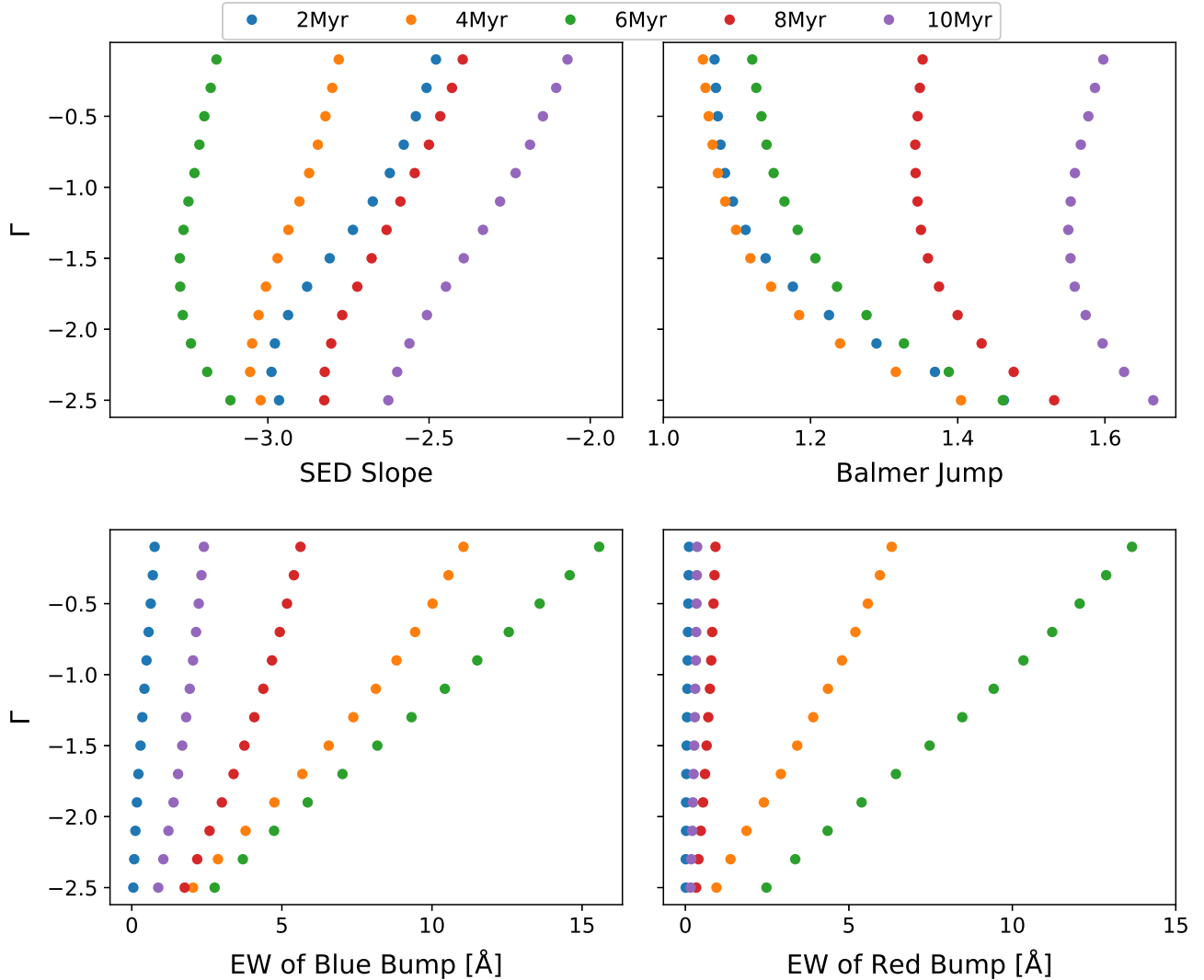


Figure 3. Variations of spectral features obtained from the synthetic integrated spectra of model clusters with a total mass of $\log M_{cl} = 6.0$ and the Solar metallicity. In the lower panels, the equivalent widths of blue and red bumps are obtained from the output of `STARBURST99`, N III $\lambda 4640 +$ C III $\lambda 4650 +$ He II $\lambda 4686$ and C IV $\lambda 5808$, respectively.

stellar clusters in external galaxies. To this end, we adopted the synthetic model `STARBURST99` (Leitherer et al. 1999, 2014) because of three reasons. First, it is possible to parameterize the underlying IMFs. This is the key option for the purpose of our survey. Second, `STARBURST99` adopts the latest evolutionary models for very massive stars up to $120 M_{\odot}$ that take into account the effects of rotation on stellar evolution. Third, the synthetic model is constantly being improved, including new spectral libraries, new stellar atmospheric grids, supernova yields, etc.

In this study, we used the `GENEVA` stellar evolutionary models adopting a rotation rate v_{ini}/v_{break} of 0.4 for the Solar ($Z = 0.014$) and sub-Solar ($Z = 0.002$) metallicities (Ekström et al. 2012; Georgy et al. 2013). Instantaneous star formation was considered as the star

formation law for YMCs. The cluster masses ranged from 3 to 8 with an interval of 0.1 dex in the logarithmic scale ($\log M_{cl}$). Stellar masses were generated in a range of $0.1 M_{\odot}$ to $120 M_{\odot}$. The frame of the underlying IMFs was adopted from the Kroupa IMF (Kroupa 2001), which is described by two power-law indices in two mass regimes: $0.1\text{--}0.5 M_{\odot}$ and $0.5\text{--}120 M_{\odot}$. We varied the power-law index Γ (or $1 - \alpha$) for the higher mass regime from 0.0 to -2.5 in 0.1 steps. Cluster ages were considered from 1 Myr to 15 Myr in 0.5 Myr intervals. The default settings were used for the other options. A total of 153,816 high resolution spectra were generated for all setups. These synthetic spectra cover a wide spectral range from 3000 \AA to 7000 \AA . Finally, we degraded the spectral resolution of the synthetic spectra to that of the

GMOS spectra ($R \sim 1700$) using SPECTRUM/SMOOTH2³ (Gray & Corbally 1994).

We analyzed the synthetic spectra generated from STARBURST99 to find spectral features that depend on the age of clusters and the underlying IMFs. The continuum spectral energy distribution (SED) of an integrated spectrum may be related to the content of massive stars. We measured the SED slopes of all synthetic spectra in the wavelength range from 4100 to 5700 Å on a logarithmic scale using a least-square fitting method. The upper left panel of Figure 3 displays the relation between the SED slope and the power-law index Γ . The SED slope shows a smooth variation with the underlying IMFs at a given cluster age.

The Balmer jump is a spectral feature related to the cluster age and underlying IMF. The integrated spectra of older clusters may have stronger Balmer jumps than those of younger clusters, because they contain more later-type stars. The strength of the Balmer jump is also related to the number ratios of O-type stars and later-type stars indicating the IMFs. We measured the strength of the Balmer jump from the synthetic spectra. In this study, the ratio of the pseudo-continuum flux and the actual flux between 3650 and 3690 Å was defined as the strength of the Balmer jump. The upper right panel of Figure 3 shows the trend between the Balmer jump and power-law index Γ as expected.

The YMCs younger than 8 Myr contain Wolf-Rayet stars. These massive evolved stars show characteristic spectral features originating from their winds in the optical passbands (Gray & Corbally 2009). The blue bump is the broad emission band composed of the blended N III $\lambda 4634-41$ and He II $\lambda 4686$ emission lines, and the red bump is characterized by C IV $\lambda 5808$. We obtained the equivalent widths (EWs) of the blue and red bumps from the output of STARBURST99 for different cluster ages and underlying IMFs (the lower panels of Figure 3). The blue bump is measurable for the first 8 Myr, while the red bump attenuates after 6 Myr. The two bumps appear to be getting stronger as the IMF becomes more top-heavy type ($\Gamma > -1.3$).

These spectral features correlate with the underlying IMFs for a given age, but there is a degeneracy between the ages and the underlying IMFs for the same measure of given spectral features. Constraining cluster ages independently may mitigate this degeneracy.

3. RESULTS

3.1. Age estimation from spectral lines

The evolutionary states of the most luminous stars in a given cluster determine the integrated spectral features. Therefore, several spectral lines associated with these stars can be used as age indicators. Figure 4 displays the synthetic spectra of the model clusters with a total stellar mass of $10^6 M_{\odot}$ generated from STARBURST99. We applied different underlying IMFs and ages to the individual model clusters for the Solar metallicity, as shown in the figure.

The upper panel of Figure 4 shows the integrated spectra with respect to the ages of the model clusters for the same underlying IMF ($\Gamma = -1.3$). The most prominent features are the blue and red bumps at around 4686 Å and 5808 Å, respectively. These emission bands appear the strongest at 4-5 Myr and gradually weaken as the cluster ages become older, making them crucial for distinguishing clusters younger than 8 Myr. By contrast, the neutral He absorption lines (He I $\lambda\lambda 4026, 4387, 4471$) as well as the two metallic lines O II $\lambda 4416$ and Mg II $\lambda 4481$ appear to be stronger for older clusters.

The lower panel displays the synthetic spectra of the model clusters with different underlying IMFs at 4 Myr. The intensities of spectral lines depend on the underlying IMFs, but the spectral variation with the cluster ages is more pronounced than the variation of the IMFs. Thus, it is possible to constrain the ages of clusters based on their spectral features. We estimated the ages of the observed clusters from the criteria summarized as below:

1. $\lesssim 2$ Myr : Weak spectral lines
2. 3 – 4 Myr : Weak He I lines, the absence of metallic lines, and the strongest Wolf-Rayet features (red and blue bumps)
3. 5 – 6 Myr : Metallic lines (O II $\lambda 4416$ and Mg II $\lambda 4481$) but weaker than He I $\lambda\lambda 4387, 4471$, and the weak Wolf-Rayet features
4. > 8 Myr : Mg II $\lambda 4481$ comparable to the adjacent He I lines and disappearance of the blue and red bumps

Figure 5 shows the normalized spectra of the observed clusters. The two clusters IDs 01 and 02 show weak blue and red bumps, and the presence of He I as well as metallic lines is evident. Therefore, they are likely older than 6 Myr but younger than 8 Myr. On the other hand, the spectra of the other five clusters (IDs 03, 08, 09, 11, and 12) are characterized by the blue and red bumps, indicating that these clusters are younger than 6 Myr.

The spectrum of ID 03 shows three detectable absorption lines O II $\lambda 4416$, He I $\lambda 4471$, and Mg II $\lambda 4481$. C III $\lambda 5696$ is stronger than the blue bump, which implies that in this cluster, WC stars are more abundant

³ <https://www.appstate.edu/~grayro/spectrum/spectrum.html>

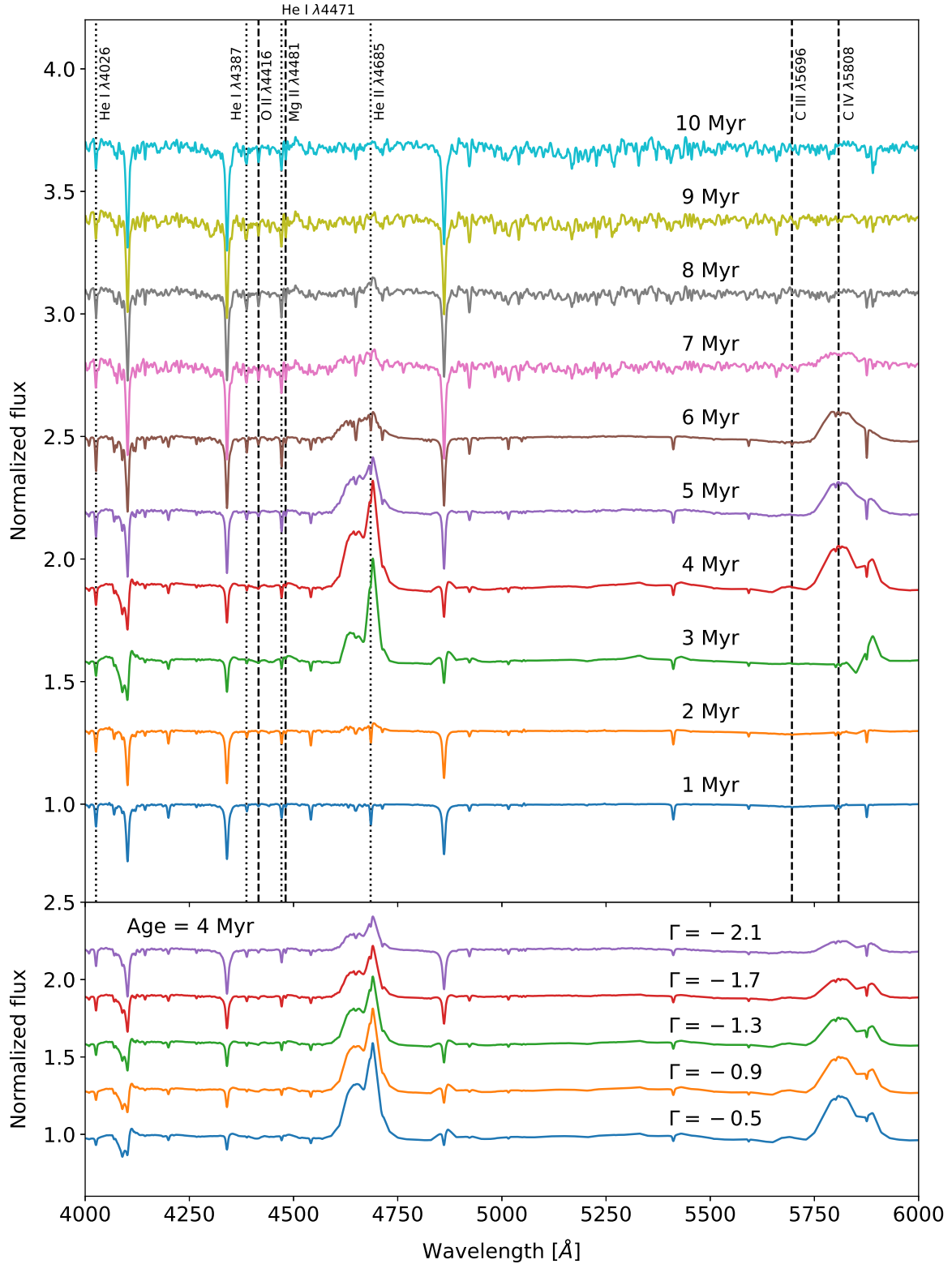


Figure 4. Synthetic spectra of the model clusters ($10^6 M_{\odot}$) with different ages (upper) and underlying IMFs (lower) for the Solar metallicity. The adopted ages and the power-law indices of the underlying IMFs are shown at the top of each spectrum. In the upper panel, several He and metallic lines related to the ages of clusters are shown as the dotted and dashed lines, respectively.

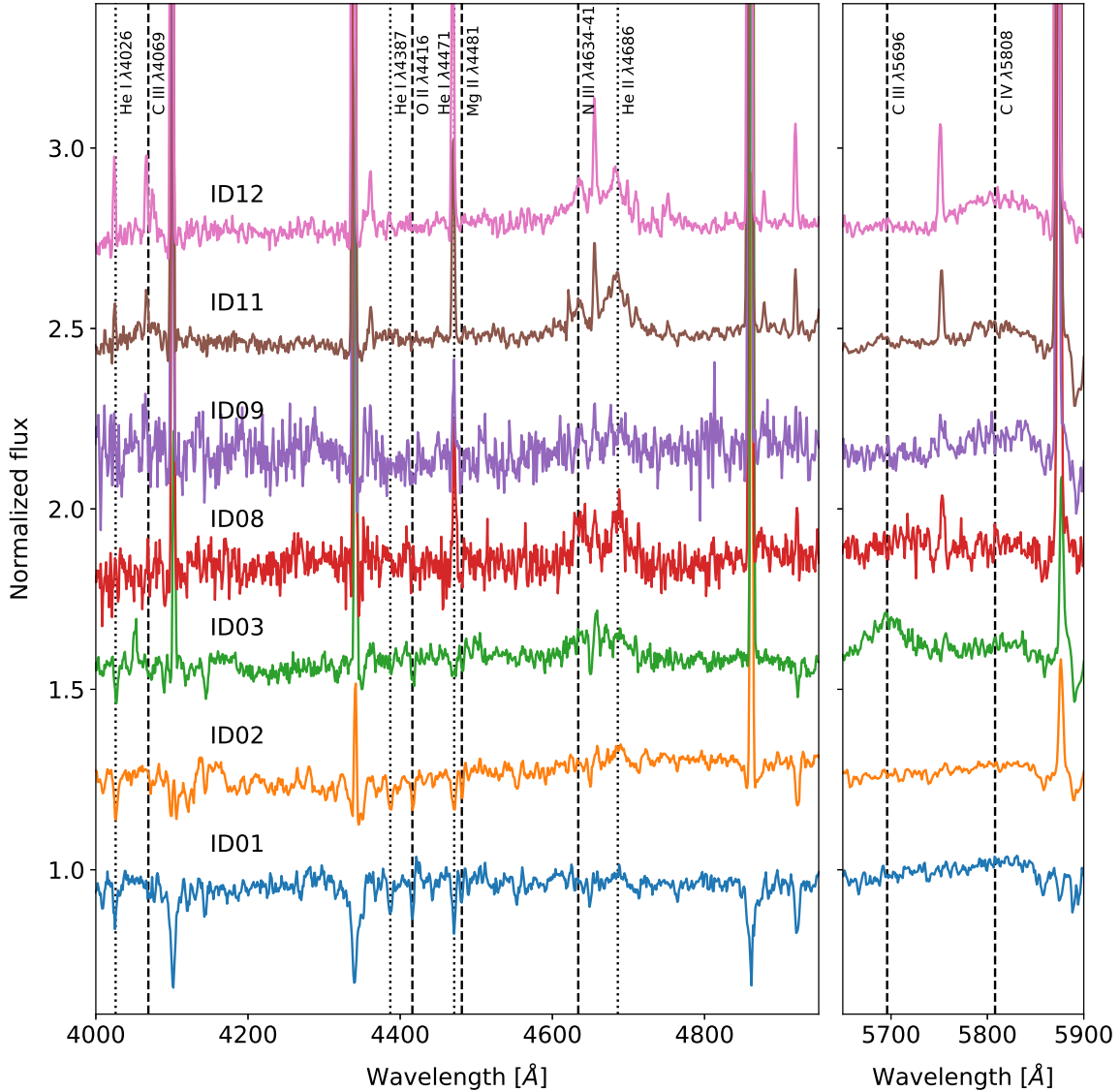


Figure 5. Spectra of the observed clusters in two spectral windows (left and right). The IDs of the individual clusters are labeled in the upper left corner of each spectrum. The spectral lines used for the age estimation are displayed in the same way as shown in Figure 4.

than WN stars (Gray & Corbally 2009). Considering that the marginal timescale on which WC-type stars can be found is between about 6 and 7 Myr (Georgy et al. 2012), the age of ID 03 is likely in this timescale.

The spectra of IDs 08, 09, 11, and 12 do not show detectable absorption lines of He I $\lambda 4387$, O II $\lambda 4416$, and Mg II $\lambda 4481$, which can be intrinsically weak. We introduced some noise into the synthetic spectra for 3 and 5 Myr-old clusters, considering the SNRs of the observed spectra. Indeed, no absorption line was detected in the synthetic spectra with SNRs similar to the observed ones. These clusters are thus likely younger than 5 Myr.

The spectra of IDs 09, 11, and 12 show a stronger red bump than C III $\lambda 5696$, which suggests the presence of early-type WC stars. In the spectra of IDs 11 and 12, the intensities of He II $\lambda 4686$ are higher than those of N III $\lambda 4634-41$ in the blue bump. This implies that the ages of these two clusters are about 3–4 Myr. We estimated the age of ID 09 to be approximately 2 Myr, given the blue bump weaker than those of IDs 11 and 12. ID 08 does not show the red bump, and the intensity of He II $\lambda 4686$ is comparable to that of N III $\lambda 4634-41$ in the blue bump. In addition, there is no detectable He and metallic absorption line. Therefore, ID 08 seems to be younger than 6 Myr but older than 4 Myr.

The nebulosity around the YMCs supports our claim that the observed clusters are indeed young. The detection of several forbidden emission lines, such as [Fe III] λ 4658, [O III] λ 4959, 5007, and [N II] λ 5755, and the strong Balmer emission lines ($H\beta$, $H\gamma$, and $H\delta$) implies the presence of hot gas. These emission lines are, in general, found in the cavities and the ridges of H II regions (Osterbrock et al. 1992; Lim et al. 2018). The origin of the observed emission lines is also related to H II regions around the YMCs. The centers of the Balmer lines are shifted away from those of the absorption lines, which is likely due to the expansion of the H II regions (Lim et al. 2018). The YMC ID 01 does not show strong emission lines. We checked the public data cube taken with the Multi Unit Spectroscopic Explorer ⁴ (MUSE). The MUSE image covering the $H\alpha$ emission line reveals that this YMC seems to be spatially associated with a giant H II region (see also the knot G in the figure 1 of Gómez-González et al. 2021). Since the sky region in the GMOS slit only covers the cavity of the giant H II region, the Balmer emission lines appears to be weak. We confirmed that the weak $H\beta$ emission was removed from our spectrum after sky subtraction.

The left panel of Figure 6 compares the ages estimated by the spectral features in this study (blue arrows) with the estimates of Whitmore et al. (2010). The age of the clusters was found to be similar on average to the previous estimate, with a standard deviation of about 1.6 Myr.

3.2. Reddening

The light from young stellar clusters in NGC 4038/9 is obscured by the interstellar medium within the Galaxy as well as their host galaxies. We adopted the mean reddening of $E(B-V) = 0.04$ toward NGC 4038/9 from the Galactic reddening map (Schlegel et al. 1998; Schlafly & Finkbeiner 2011). A total extinction of $A_V = 0.12$ mag was adopted by assuming the mean total-to-selective extinction ratio of $R_V = 3.1$. We note that the reddening map of Schlafly & Finkbeiner (2011) was re-calibrated by a factor of 0.86 from their previous reddening map (Schlegel et al. 1998). This study adopted the more recent $E(B-V)$ scale of Schlafly & Finkbeiner (2011).

The strength of the Na I D lines is a useful tool to estimate the internal extinction of external galaxies. We adopted different empirical relations between extinction and the EWs of the Na I D lines, because the line strength nonlinearly increases with interstellar reddening (Poznanski et al. 2012; Murga et al. 2015). The rela-

tions of Murga et al. (2015) and Poznanski et al. (2012) were applied to the less reddened cases [$E(B-V) \leq 0.08$] and more reddened cases [$E(B-V) > 0.08$], respectively. We identified the Na I D lines in the observed spectra, but the spectral resolution of our spectra was insufficient to directly measure the individual line strengths. The internal reddening of the individual clusters was estimated by comparing the modeled Na I D lines with the observed ones.

Based on the empirical relations of the two previous studies (Poznanski et al. 2012; Murga et al. 2015), we computed the EWs in the $E(B-V)$ range of 0.01 to 1.2 with an interval of 0.01. The Na I D lines were modeled from the computed EWs, where the line profiles were assumed to be Gaussian. Instrumental broadening was applied to the modeled line profiles. These modeled lines were then subtracted from the observed Na I D lines. We adopted $E(B-V)$, which shows the minimum rms value of the residuals. Since the reddening values of Poznanski et al. (2012) and Murga et al. (2015) were scaled to those of Schlegel et al. (1998), the $E(B-V)$ that we obtained were multiplied by 0.86. The propagated errors in the uncertainties of the two empirical relations were adopted as the errors of the reddening.

Na I D lines form in the atmospheres of late-type stars, and therefore, these lines can be found in the spectra of older clusters. We investigated the spectra obtained from STARBURST99 (Leitherer et al. 1999, 2014) and found Na I D lines for the clusters older than 7 Myr. Hence, the line strengths are associated with both reddening and the ages of clusters. Since the ages of the observed YMCs are younger than or close to 7 Myr, the contribution of the stellar absorption line to the EW of the interstellar Na I D line may be negligible. The middle panel of Figure 6 compares the $E(B-V)$ values from this study measured by the Na I D lines (blue crosses) with those of Whitmore et al. (2010). Our estimates are on average lower than theirs by 0.05. Bastian et al. (2009) also derived a reddening of about 0.10 toward ID 03 (T352), which is 0.05 smaller than our result.

3.3. Spectral matching

We compared the observed spectra with a grid of the synthetic spectra generated from STARBURST99 (Leitherer et al. 1999, 2014) to derive the physical parameters of the individual clusters such as age, reddening, cluster mass, and the underlying IMF. The radial velocities of the individual clusters were measured using H and He lines. The centers of these lines were obtained from the best-fit Gaussian profiles, and the radial velocities of the lines were calculated. The mean values

⁴ <http://archive.eso.org/cms.html>

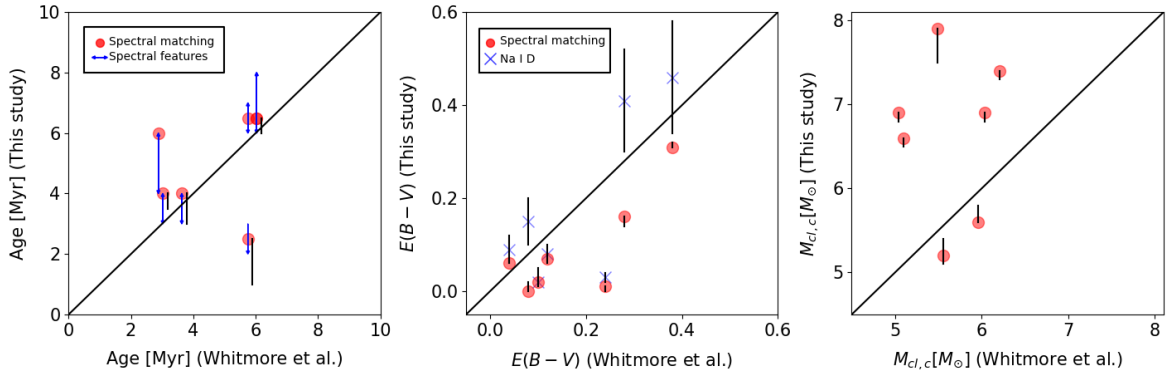


Figure 6. Comparison of the parameters derived in this study with the results from [Whitmore et al. \(2010\)](#). The diagonal solid lines represent one-to-one relations for given parameters. The left panel compares the ages from the previous study with ours. The blue arrows indicate the age ranges estimated from the spectral features, and the red dots denote the ages inferred from the spectral matching. The middle panel shows a comparison of the reddening values. The blue crosses and red dots represent the results obtained from the Na I D lines and spectral matching, respectively. The vertical lines represent the errors on each parameter. The current masses of the YMCs estimated from this study are compared with those from the previous study in the right panel.

were adopted as the radial velocities of the individual clusters.

We reduced the large grid of the synthetic spectra to a smaller set in the expected age range of given clusters. The fluxes of the synthetic spectra were computed by dividing the luminosities of the spectra by $4\pi d^2$, where d is the adopted distance of 22 Mpc ([Schweizer et al. 2008](#)). These fluxes were then reddened by the internal extinction of the host galaxies using the Galactic extinction curve ([Fitzpatrick 1999](#)) with an R_V of 3.1 ([Guetter & Vrba 1989](#)), where the reddening estimated from the Na I D lines was used for the internal extinction. We shifted the reddened synthetic spectra to the observed wavelength frame using the radial velocities and applied the mean Galactic reddening to the spectra.

For spectral matching, the χ^2 values between the observed and synthetic spectra were computed in a full wavelength range. Strong H and He lines as well as nebular lines were masked out in the spectral fitting procedure. In particular, the nebular lines introduce slightly larger errors in the χ^2 minimization because the synthetic spectra do not include such emission lines. The Balmer jump and the two bumps are key features in the determination of the underlying IMFs, and therefore, three spectral windows covering these features were weighted in the χ^2 calculation. We probed the χ^2 values adjusting the internal extinction at a given age. This iterative process was extended to the ranges of the ages estimated from the spectral features (Section 3.1).

The synthetic spectra were sorted in decreasing order of χ^2 value. We visually inspected the top three spectra with the minimum χ^2 . The synthetic spectra with the smallest χ^2 values were adopted as the best-fit spectra, but in some cases (IDs 09 and 11) these spectra did

not best match the two bumps. In such cases, we selected the synthetic spectra with the smallest χ^2 values for the two bumps among the top three models. The top three models yield nearly consistent parameters of the observed clusters. The upper and lower bounds in age, reddening, cluster mass, and the IMF from the top three models were adopted as the errors of the individual parameters (vertical lines in Figure 6). Figure 7 shows the spectra that best fit the observed spectra. We summarized the physical parameters of the YMCs in Table 1.

Figure 6 compares the parameters of the observed clusters obtained by different methods. In the left panel, the ages obtained from the spectral matching (red dots) naturally overlap with the age ranges estimated from the spectral features (blue arrows), since the best-fit synthetic spectra were searched for in the expected age ranges. Therefore, our estimates are, on average, similar to the results of [Whitmore et al. \(2010\)](#) for the same clusters. In the middle panel, the spectral matching technique (red dots) tends to yield smaller reddening than those obtained from the Na I D lines (blue crosses), and also smaller than the reddening of [Whitmore et al. \(2010\)](#).

Spectral matching yields the initial masses of the individual clusters because `STARBURST99` does not give the current masses of clusters. From the initial masses, we estimated the current masses ($\log M_{cl,c}$) using the Monte-Carlo technique. A large number of artificial stars were generated in a mass range from $0.1 M_\odot$ to $120 M_\odot$, where the IMFs obtained from the spectral matching were adopted as the underlying IMFs of the individual clusters. The Geneva stellar evolutionary models for the Solar metallicity ([Ekström et al. 2012](#)) were used to

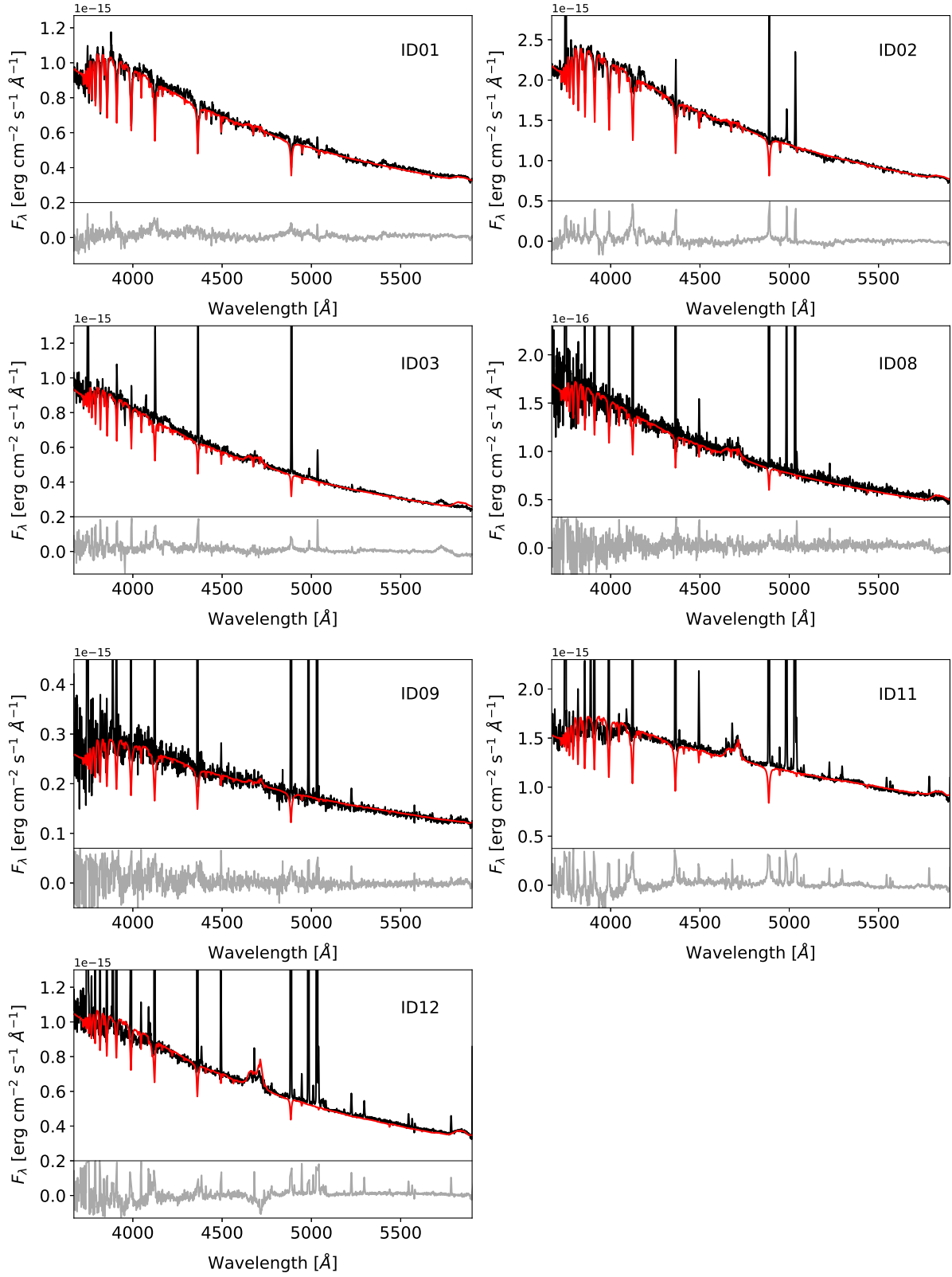


Figure 7. Comparison of the observed spectra (black) with the best-fit synthetic spectra (red). The residual for the difference between the observed and synthetic spectra is shown below the horizontal line in each panel.

consider the mass loss due to stellar evolution at given ages. This simulation was repeated 100 times.

As a result, the YMCs still appears to have current masses comparable to their initial masses in a logarithmic scale ($\log M_{cl,i} \approx \log M_{cl,c}$). The effect of stellar evolution on the cluster masses is less than 1%, except for the two YMCs IDs 03 and 08. The right panel of Figure 6 compares the current masses of the YMCs from two studies, showing that 70% of the YMCs in this study have significantly higher masses than those from Whitmore et al. (2010) by more than one order of magnitude. In the extreme case, the difference is larger than two orders of magnitude. We discuss the possible causes of the systematic differences in later section. The mass of ID 03 ($\log M_{cl,c} = 5.6$) is in good agreement with the results of Bastian et al. (2009); however, we obtained a significantly smaller internal reddening [$E(B - V) \sim 0$] compared to their result and a shallow IMF ($\Gamma = -1.0$).

Most underlying IMFs inferred from the integrated spectra of the observed YMCs appear to deviate from the Salpeter/Kroupa IMF (Salpeter 1955; Kroupa 2001). Interestingly, we also found a correlation between the cluster masses and the power-law indices Γ , as plotted in Figure 8. The masses of stars in more massive clusters are drawn from the IMF with smaller Γ , i.e. the bottom-heavy IMF. Given the small differences in the fundamental parameters among the top three models, the wide range of Γ values is unlikely due to the uncertainties from the analysis. Therefore, our result gives an implication that adopting a universal form of the IMF may not always be valid. By contrast, this trend appears to be weaker in the correlation between the cluster masses estimated by Whitmore et al. (2010) and Γ obtained in this study (triangles).

4. DISCUSSION

The fundamental parameters of seven YMCs in NGC 4038/9 were derived by comparing their integrated spectra with those synthesized from a simple stellar population model. As a result, our results suggest a variation of the stellar IMFs. Here, we discuss the several sources that can cause uncertainties in our analysis. The first source is the SNR of a given spectrum. A low SNR can blur spectral features, increasing the uncertainty in derived physical parameters. To investigate the effects, we introduced random errors corresponding to final SNRs into the synthetic spectra that best matched the observed spectra, and then retrieved the physical parameters of YMCs from the noise-added spectra. This simulation was repeated 100 times. As a result, small errors

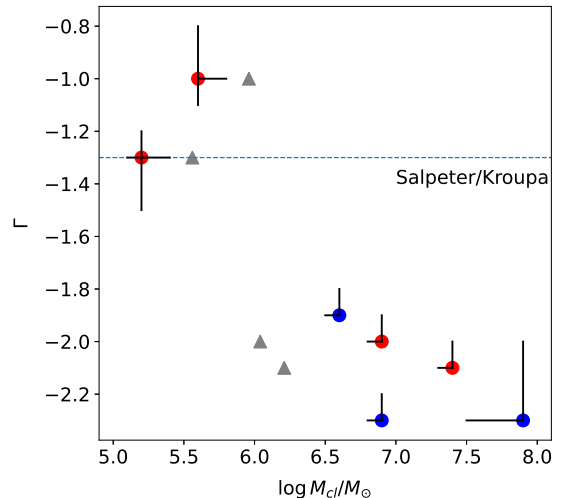


Figure 8. Correlation between the cluster masses and Γ of the underlying IMFs. The red and blue dots represent the spatially well-isolated YMCs and the blended YMCs with nearby sources, respectively. The triangle shows the relationship between the cluster masses from Whitmore et al. (2010) and the underlying IMFs from this study for the isolated YMCs. The vertical and horizontal lines indicate the upper and lower bounds of cluster masses and Γ obtained from the spectral matching. The horizontal line represents the Γ value of $= -1.3$ for the Salpeter/Kroupa IMF.

(0.1 dex in $\log M_{cl,i}$ and 0.1 in Γ) occurred only for ID 08 with SNR of 25. Therefore, the SNR may not introduce large errors on the physical parameters of YMCs.

The second source is reddening correction. The internal reddening obtained from the Na I D line tends to be larger than that from spectral matching. One possibility for this difference is that the strength of the Na I D line is not a precise reddening tracer. Indeed, there is a weak correlation between the Na I and H I column densities due to the large scatter in the derived column densities (Murga et al. 2015). The diffuse interstellar band (DIB) at 5780 Å traces the reddening fairly well (Herbig 1993; Friedman et al. 2011; Lan et al. 2015), and there is a good correlation between the strength of the DIB $\lambda 5780$ and the Na I column density. However, the relationship between the strength of the DIB and reddening as well as the H I column density does not appear to hold for strong ultraviolet radiation fields (Friedman et al. 2011; Welty 2014). If the behavior of Na I is similar to that of the DIB $\lambda 5780$, the Na I D line may not precisely trace reddening toward the YMCs containing a number of ionizing sources.

The spectra of the YMCs are reddened with $E(B - V)$ ranging from 0.02 to 0.46 in addition to the Galactic reddening. The correction for the internal reddening is complicated. The light from the individual YMCs is obscured by the diffuse interstellar medium in their host

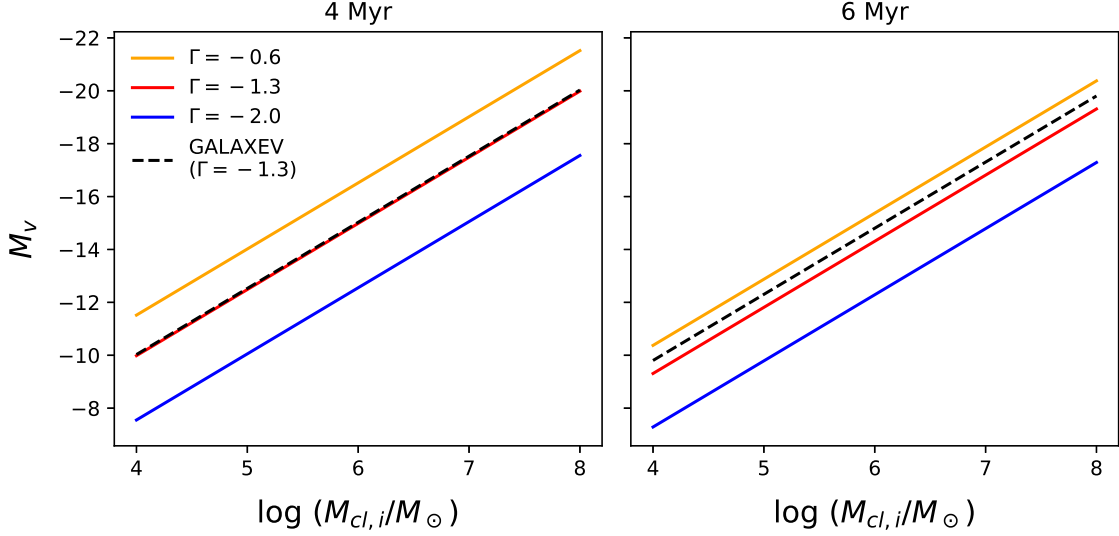


Figure 9. Initial mass-luminosity relations with three different underlying IMFs ($\Gamma = -0.6, -1.3,$ and -2.0) at 4 and 6 Myr. These relations were obtained from **STARBURST99** for the Solar metallicity. The adopted stellar evolution models consider the effects of rotation on stellar evolution (Ekström et al. 2012). The dashed line represents the initial mass-luminosity relation from **GALAXEV** (Bruzual & Charlot 2003) for the Kroupa IMF.

Table 1. Physical properties of seven YMCs in NGC4038/9

ID	V	$E(B - V)_{\text{Na I}}$	$E(B - V)_{\text{mat}}$	Age _{spec} [Myr]	Age _{mat} [Myr]	log $M_{cl,i}$	log $M_{cl,c}$	Γ	SNR	Whitmore ID
01	17.57	0.09 (0.03)	$0.06^{+0.01}_{-0.00}$	6–8	$6.5^{+0.0}_{-0.5}$	$6.9^{+0.0}_{-0.1}$	6.9	$-2.0^{+0.1}_{-0.0}$	40	50776
02	16.66	0.08 (0.02)	$0.07^{+0.01}_{-0.00}$	6–8	$6.5^{+0.0}_{-0.5}$	$7.4^{+0.0}_{-0.1}$	7.4	$-2.1^{+0.1}_{-0.0}$	80	36094
03	17.83	0.15 (0.05)	$0.00^{+0.02}_{-0.00}$	6–7	6.5	$5.7^{+0.1}_{-0.1}$	5.6	$-1.0^{+0.2}_{-0.1}$	80	38220(38377, 38305, and 38195)
08	19.55	0.03 (< 0.01)	$0.01^{+0.00}_{-0.01}$	4–6	6.0	$5.2^{+0.2}_{-0.1}$	5.2	$-1.3^{+0.1}_{-0.2}$	25	55784
09	18.62	0.41 (0.11)	$0.16^{+0.00}_{-0.02}$	2–3	$2.5^{+0.0}_{-1.5}$	$6.9^{+0.0}_{-0.1}$	6.9	$-2.3^{+0.1}_{-0.0}$	45	22079(22109)
11	16.34	0.46 (0.12)	$0.31^{+0.01}_{-0.00}$	3–4	$4.0^{+0.0}_{-0.5}$	$7.9^{+0.0}_{-0.4}$	7.9	$-2.3^{+0.3}_{-0.0}$	60	15502(15492 and 15466)
12	17.22	0.02 (< 0.01)	$0.02^{+0.03}_{-0.00}$	3–4	$4.0^{+0.0}_{-1.0}$	$6.6^{+0.0}_{-0.1}$	6.6	$-1.9^{+0.1}_{-0.0}$	90	19459(19416, 19374, 19435, and 19394)

NOTE—Column (1) : Cluster ID. Column (2) : V magnitude from synthetic photometry. Columns (3) and (4) : Reddening estimated from the Na I D line and the spectral matching. Columns (5) and (6) : Ages estimated from the spectral features and the spectral matching. Columns (7) and (8) : The initial cluster mass and current cluster mass in a logarithmic scale. Column (9) : The power law index Γ of the IMF. Column (10) : Signal-to-Noise Ratio. Column (11) : The IDs from Whitmore et al. (2010). The numbers in parentheses represent the IDs of neighboring sources.

galaxies as well as the remaining natal clouds (or intra-cluster medium). Although the contribution of the diffuse interstellar medium in NGC 4038/9 to the internal reddening may not be high as these host galaxies have a face-on morphology, the natal clouds still contain a large fraction of dust grains. Furthermore, the inhomogeneous distribution of dust grains across the remaining clouds results in differential reddening. It is practically impossible to correct for differential reddening in the integrated spectra of unresolved stellar systems. Therefore, some of the differences between the observed and best-matched spectra may be related to differential reddening.

The Galactic mean R_V was adopted for calculating the internal extinction A_V . This R_V can also result in systematic uncertainties in our analysis. A number of photometric studies have confirmed that the abnormal reddening law deviates from the Galactic mean R_V for very young active star-forming regions in the Galaxy, e.g., the Orion Nebula Cluster (Johnson 1967; Cardelli et al. 1989; Da Rio et al. 2016), Carina Nebula (Hur et al. 2023), Westerlund 2 (Hur et al. 2015), NGC 281 (Kim et al. 2021), NGC 6530 (Fernandes et al. 2012), and NGC 6611 (Chini & Wargau 1990).

However, there is a tendency that open clusters older than 3 – 5 Myr do not show the abnormal reddening

law, e.g., IC 1848 (Lim et al. 2014), IC 1805 (Guetter & Vrba 1989; Sung et al. 2017), and NGC 6231 (Sung et al. 2013). In particular, the R_V in the Carina Nebula shows a clear spatial variation with respect to the age of young clusters (Hur et al. 2023). Anomalous extinction is found for young open clusters Trumpler 14, 16, and Collinder 232 in the southern Carina Nebula, but R_V becomes normal for the older cluster Trumpler 15 in the northern region. These facts imply that the timescale for the evolution of dust grains in size is approximately 3 – 5 Myr, and it may also depend on the amount of ultraviolet radiation flux and the metallicity of star-forming regions.

With the exception of ID 09, the observed YMCs are older than 4 Myr, and therefore, the R_V toward these clusters is thought to be normal. Even if anomalous extinction affects the integrated light from the YMCs, the effect on our results would not be severe. The increase in R_V due to dust growth mitigates the effect of wavelength-dependent selective extinction in optical passbands (Fitzpatrick 1999). For a quantitative test, we applied an R_V of 5 to the spectra of ID 11 with the largest $E(B - V)$ and searched for the best-matched synthetic spectra. This resulted in a small change in the fundamental parameters of the YMC: an age of 0.5 Myr, a logarithmic cluster mass of 0.1 dex, and a power-law index of 0.3.

The third source is the adopted metallicity. The synthetic spectra generated from a simple stellar population model for the Solar metallicity were matched to the observed spectra. We found no evidence that the YMCs have different metallicity from the Solar value. Synthetic spectra for sub-Solar metallicity ($Z = 0.002$) were compared with the observed spectra, but none of the synthetic spectra fit the Wolf-Rayet bumps. This result is consistent with the observation that the Wolf-Rayet wind is weaker in low-metallicity environments (Crowther & Hadfield 2006). Chemical analyses from previous studies also support our claim. Bastian et al. (2009) analyzed the integrated spectra of several stellar clusters in NGC 4038/9 and found that these clusters have the Solar metallicity. Gómez-González et al. (2021) also confirmed the Solar metallicity from the oxygen abundance of Wolf-Rayet stars in the same galaxies.

The fourth source is the degeneracies among the physical parameters of YMCs. Since the integrated spectral features depend on the cluster age and the underlying IMF, as shown in Figure 3, our results can still be affected by the degeneracies between the two parameters. There are possibly multiple models explaining the observed spectra. We tested the possibility that the stellar population in the observed YMCs is drawn from the

Salpeter/Kroupa IMF. A simple manner to do this is to apply the fundamental parameters derived by Whitmore et al. (2010) to the synthetic spectra and compare them with the observed spectra, because they analyzed the photometric data by means of a simple stellar population model adopting the Salpeter/Kroupa IMF. However, there is no synthetic spectrum that matches the observed spectra in both stellar evolution models with and without rotation.

For the five YMCs with the bottom-heavy IMFs, we adopted the Salpeter/Kroupa IMF as the underlying IMF and examined the best-matched synthetic spectra in the ranges of ages and reddening values. However, the newly matched synthetic spectra do not fit the Balmer jumps or the overall slope of the observed spectra any better than the synthetic spectra with the bottom-heavy IMFs. Therefore, our results may not originate from the degeneracies between the age and the underlying IMF.

The fifth source is the blending effect with neighboring objects. The masses of five YMCs are significantly larger than those estimated by Whitmore et al. (2010). Since these YMCs occupy the high-mass regime in the cluster mass-IMF correlation (Figure 8), the reliability of the derived cluster masses should be scrutinized. We confirmed that three YMCs (IDs 09, 11, and 12) have at least one bright neighboring source in the high-resolution HST images. Since these sources were not resolved in our seeing-limited pre-image, the integrated fluxes of these YMCs are likely overestimated compared to those from Whitmore et al. (2010), leading to the high cluster masses. In fact, the V magnitudes of these three YMCs obtained from the synthetic photometry are smaller (brighter) than those of the previous study. If the individual YMCs and their neighboring sources are part of stellar associations or complexes, it is possible that we have inferred the masses and the underlying IMFs of such large-scale stellar systems.

On the other hand, the other two YMCs (IDs 01 and 02) are spatially well-isolated without bright neighboring sources. In addition, their brightness in the V band are comparable to the previous measurements. We examined the systematic error originating from the adopted stellar population models as the sixth source. Figure 9 shows a comparison of the mass-luminosity relations from STARBURST99 (red solid line – Leitherer et al. 1999, 2014) and GALAXEV (black dashed line – Bruzual & Charlot 2003) for the Kroupa IMF. At 4 Myr, the two relations are almost the same, while the cluster masses estimated from GALAXEV are 0.2 dex smaller than those from STARBURST99 for a given luminosity at 6 Myr. There are systematic differences between the mass-luminosity relations from the two models, but the

systematic errors associated with the adopted models are insufficient to explain the significant mass differences between the previous study and ours for the two clusters.

We suggest that the differences in cluster masses may be attributed to the different underlying IMFs. Figure 9 displays the mass-luminosity relations for three different underlying IMFs (orange, red, and blue solid lines) at 4 and 6 Myrs. Younger clusters tend to be more luminous than their older counterparts for the same masses. At the same age, the clusters with the bottom-heavy IMFs are less luminous than the clusters with the shallower IMFs. Therefore, there are several possibilities for inferring cluster masses from a given luminosity.

Whitmore et al. (2010) estimated the physical parameters of clusters by comparing the integrated broadband photometric data with those predicted from the adopted stellar population model. Here, we emphasize that the broadband photometry is insensitive to the spectral features related to the IMFs. There are, thus, degeneracies among cluster ages, underlying IMFs, and cluster masses. We have shown that cluster ages and underlying IMFs can be constrained by probing the variation of spectral features and comparing them with the synthetic ones. Spectral analysis can provide a better estimate of the cluster mass.

The YMC ID 02 is the most massive star cluster ($2.5 \times 10^7 M_{\odot}$) among the four isolated YMCs. The large amount of line broadening due to the rapid rotation of massive stars hinders the estimation of the dynamical mass of this cluster. The assumption of this dynamical mass estimation is that a given cluster is in a virial state, which does not hold for very young clusters. We surveyed the literature to determine whether our estimate is acceptable within the upper bound of the cluster mass. The upper limit of star clusters is known to be about $\lesssim 10^8 M_{\odot}$ (Norris et al. 2019). Indeed, the dynamical mass of W3 in NGC 7252 were estimated to be $8.0 \times 10^7 M_{\odot}$ (Maraston et al. 2004). Bastian et al. (2006) reported that the total masses of two individual clusters G114 in NGC 1316 and W30 in NGC 7252 exceed $10^7 M_{\odot}$. Given the old ages of these clusters, their initial masses may be about $10^8 M_{\odot}$. Renaud et al. (2015) performed hydrodynamic simulations of star cluster formation in merging galaxies such as NGC 4038/9 and found significantly massive clusters with total stellar masses up to $\sim 10^8 M_{\odot}$. The results of these previous studies support that the mass of the YMC ID 02 is acceptable.

We have discussed the impacts of several sources and assumptions such as reddening, the adopted metallicity, stellar population models, and the degeneracy among the fundamental parameters on our results. There are

practical limitations in the proper correction for the differential reddening; however, it is difficult to quantitatively infer the uncertainty due to this effect. On the other hand, the other sources and assumptions do not severely change our results. We caution about the blend of multiple sources in the seeing-limited images. The YMC IDs 09, 11, and 12 in our sample are subject to blending of neighboring sources. Nevertheless, the correlation between the masses and the underlying IMFs of the other YMCs still appears to hold (Figure 8).

5. SUMMARY

We investigated the integrated spectra of seven YMCs in NGC 4038/9 to infer their underlying IMFs. The features of the observed spectra were interpreted by means of the simple stellar population model STARBURST99 (Leitherer et al. 1999, 2014). The fundamental parameters of the YMCs were inferred from the synthetic spectra that best matched the observed spectra.

The most prominent spectral features associated with stellar content of the YMCs are the blue and red bumps originating from Wolf-Rayet star populations. The presence of these features indicates that the YMCs are younger than 8 Myr. The ages of the YMCs estimated from the best-matched synthetic spectra range from 2.5 Myr to 6.5 Myr, which is on average similar to the results of Whitmore et al. (2010).

The internal reddening $E(B - V)$ obtained from the Na I D lines ranges from 0.02 to 0.46. We adopted the reddening values as the initial values for spectral matching and redetermined the reddening that matches the slopes of the observed spectra. The reddening values obtained in Whitmore et al. (2010) lie between those determined by the Na I D lines and the spectral matching.

The masses of the observed YMCs are higher than $10^5 M_{\odot}$ and smaller than $10^8 M_{\odot}$. Hence, it is confirmed that they are, indeed, massive stellar clusters. The YMCs appear to have various underlying IMFs. The power-law index Γ ranges from -1.0 to -2.3 , which is equivalent to 2.0 to 3.3 in α . More massive clusters tend to have bottom-heavy IMFs. Considering these results, the implication is that the choice of the underlying IMF is crucial in analyzing unresolved stellar populations. However, several of our most massive clusters are contaminated and might have their masses overestimated, and the sample size is insufficient. A systematic survey of young stellar clusters in several external galaxies with more diverse environments will further clarify our results.

The authors thank the anonymous referee for constructive comments and suggestions. The authors would also like to express thanks to Dr. Sang-Hyun Chun and Professor Dohyeong Kim for their help. This paper has made use of data obtained under the K-GMT Science Program (PIDs: GEMINI-KR-2022A-004 and GEMINI-KR-2023A-004) supported by the Korea Astronomy and Space Science Institute (KASI) grant funded by the Korean government (MSIT; No. 2023-1-860-02, International Optical Observatory Project). This research has also made use of the SIMBAD database, operated at CDS, Strasbourg, France. This work was supported by the National Research Foundation of Korea (NRF) grant funded by the Korean government (MSIT; grant No. 2022R1C1C2004102). This research of H.-J. K. was supported by Basic Science Research Program through the National Research Foundation of Korea (NRF) funded by the Ministry of Education (RS-2023-00246733).

Facilities: Gemini South:8.1m

Software: **Astropy** (Astropy Collaboration et al. 2013, 2018, 2022), **NumPy** (Harris et al. 2020), **SciPy** (Virtanen et al. 2020), **Pyphot** (Fouesneau 2022)

REFERENCES

- Amram, P., Marcelin, M., Boulesteix, J., et al. 1992, *A&A*, 266, 106
- Astropy Collaboration, Robitaille, T. P., Tollerud, E. J., et al. 2013, *A&A*, 558, A33
- Astropy Collaboration, Price-Whelan, A. M., Sipőcz, B. M., et al. 2018, *AJ*, 156, 123
- Astropy Collaboration, Price-Whelan, A. M., Lim, P. L., et al. 2022, *ApJ*, 935, 167
- Bastian, N., Covey, K. R., & Meyer, M. R. 2010, *ARA&A*, 48, 339
- Bastian, N., Hempel, M., Kissler-Patig, M., et al. 2005, *A&A*, 435, 65
- Bastian, N., Saglia, R. P., Goudfrooij, P., et al. 2006, *A&A*, 448, 881
- Bastian, N., Tranco, G., Konstantopoulos, I. S., et al. 2009, *ApJ*, 701, 607
- Bica, E., Santiago, B. X., Dutra, C. M., et al. 2001, *A&A*, 366, 827
- Boylan-Kolchin, M. 2023, *Nature Astronomy*, 7, 731
- Brandner, W., Clark, J. S., Stolte, A., et al. 2008, *A&A*, 478, 137
- Bruzual, G. & Charlot, S. 2003, *MNRAS*, 344, 1000. doi:10.1046/j.1365-8711.2003.06897.x
- Burbidge, E. M. & Burbidge, G. R. 1966, *ApJ*, 145, 661
- Cameron, A. J., Katz, H., Witten, C., et al. 2024, *MNRAS*, 534, 523
- Cantat-Gaudin, T., Jordi, C., Vallenari, A., et al. 2018, *A&A*, 618, A93
- Cardelli, J. A., Clayton, G. C., & Mathis, J. S. 1989, *ApJ*, 345, 245
- Chini, R. & Wargau, W. F. 1990, *A&A*, 227, 213
- Clark, J. S., Negueruela, I., Davies, B., et al. 2009, *A&A*, 498, 109
- Crowther, P. A. & Hadfield, L. J. 2006, *A&A*, 449, 711
- Da Rio, N., Tan, J. C., Covey, K. R., et al. 2016, *ApJ*, 818, 59
- Davies, B., Figer, D. F., Kudritzki, R.-P., et al. 2007, *ApJ*, 671, 781
- de Grijs, R., Anders, P., Bastian, N., et al. 2003, *MNRAS*, 343, 1285
- Dias, W. S., Monteiro, H., Moitinho, A., et al. 2021, *MNRAS*, 504, 356
- Ekström, S., Georgy, C., Eggenberger, P., et al. 2012, *A&A*, 537, A146
- Espada, D., Komugi, S., Muller, E., et al. 2012, *ApJL*, 760, L25
- Fabbiano, G., Baldi, A., King, A. R., et al. 2004, *ApJL*, 605, L21
- Fabbiano, G., Krauss, M., Zezas, A., et al. 2003, *ApJ*, 598, 272
- Fernandes, B., Gregorio-Hetem, J., & Hetem, A. 2012, *A&A*, 541, A95
- Figer, D. F., Kim, S. S., Morris, M., et al. 1999, *ApJ*, 525, 750
- Fitzpatrick, E. L. 1999, *PASP*, 111, 63
- Figer, D. F., MacKenty, J. W., Robberto, M., et al. 2006, *ApJ*, 643, 1166

- Fouesneau, M. (2022). pyphot (Version 1.4.3) [Computer software]. <https://github.com/mfouesneau/pyphot>
- Friedman, S. D., York, D. G., McCall, B. J., et al. 2011, *ApJ*, 727, 33
- Gao, Y., Lo, K. Y., Lee, S.-W., et al. 2001, *ApJ*, 548, 172
- Georgy, C., Ekström, S., Eggenberger, P., et al. 2013, *A&A*, 558, A103
- Georgy, C., Ekström, S., Meynet, G., et al. 2012, *A&A*, 542, A29
- Gómez-González, V. M. A., Mayya, Y. D., Toalá, J. A., et al. 2021, *MNRAS*, 500, 2076.
- Gouliermis, D. A. 2018, *PASP*, 130, 072001
- Gray, R. O. & Corbally, C. J. 1994, *AJ*, 107, 742
- Gray, R. O. & Corbally, C. 2009, *Stellar Spectral Classification by Richard O. Gray and Christopher J. Corbally*. Princeton University Press, 2009. ISBN: 978-0-691-12511-4
- Guetter, H. H. & Vrba, F. J. 1989, *AJ*, 98, 611
- Harris, C. R., Millman, K. J., van der Walt, S. J., et al. 2020, *Nature*, 585, 357
- Herbig, G. H. 1993, *ApJ*, 407, 142. doi:10.1086/172500
- Hibbard, J. E., van der Hulst, J. M., Barnes, J. E., et al. 2001, *AJ*, 122, 2969
- Hosek, M. W., Lu, J. R., Anderson, J., et al. 2019, *ApJ*, 870, 44
- Hur, H., Lim, B., & Chun, M.-Y. 2023, *Journal of Korean Astronomical Society*, 56, 97
- Hur, H., Park, B.-G., Sung, H., et al. 2015, *MNRAS*, 446, 3797
- Hwang, N. & Lee, M. G. 2008, *AJ*, 135, 1567
- Johnson, H. L. 1967, *ApJL*, 150, L39. doi:10.1086/180088
- Kim, S., Lim, B., Bessell, M. S., et al. 2021, *AJ*, 162, 140
- Kroupa, P. 2001, *MNRAS*, 322, 231
- Lada, C. J. & Lada, E. A. 2003, *ARA&A*, 41, 57
- Lan, T.-W., Ménard, B., & Zhu, G. 2015, *MNRAS*, 452, 3629
- Leitherer, C., Ekström, S., Meynet, G., et al. 2014, *ApJS*, 212, 14
- Leitherer, C., Schaerer, D., Goldader, J. D., et al. 1999, *ApJS*, 123, 3
- Lim, B., Chun, M.-Y., Sung, H., et al. 2013, *AJ*, 145, 46
- Lim, S., Hwang, N., & Lee, M. G. 2013, *ApJ*, 766, 20
- Lim, B., Sung, H., Bessell, M. S., et al. 2018, *MNRAS*, 477, 1993. doi:10.1093/mnras/sty713
- Lim, B., Sung, H., Hur, H., et al. 2017, *Formation, Evolution, and Survival of Massive Star Clusters*, 316, 357
- Lim, B., Sung, H., Kim, J. S., et al. 2014, *MNRAS*, 438, 1451
- Maraston, C., Bastian, N., Saglia, R. P., et al. 2004, *A&A*, 416, 467
- Metz, J. M., Cooper, R. L., Guerrero, M. A., et al. 2004, *ApJ*, 605, 725
- Murga, M., Zhu, G., Ménard, B., et al. 2015, *MNRAS*, 452, 511
- Neff, S. G. & Ulvestad, J. S. 2000, *AJ*, 120, 670
- Norris, M. A., van de Ven, G., Kannappan, S. J., et al. 2019, *MNRAS*, 488, 5400
- Osterbrock, D. E., Tran, H. D., & Veilleux, S. 1992, *ApJ*, 389, 305. doi:10.1086/171206
- Porras, A., Christopher, M., Allen, L., et al. 2003, *AJ*, 126, 1916
- Poznanski, D., Prochaska, J. X., & Bloom, J. S. 2012, *MNRAS*, 426, 1465
- Renaud, F., Bournaud, F., & Duc, P.-A. 2015, *MNRAS*, 446, 2038
- Salpeter, E. E. 1955, *ApJ*, 121, 161
- Schlafly, E. F. & Finkbeiner, D. P. 2011, *ApJ*, 737, 103
- Schlegel, D. J., Finkbeiner, D. P., & Davis, M. 1998, *ApJ*, 500, 525
- Schulz, A., Henkel, C., Muters, D., et al. 2007, *A&A*, 466, 467
- Schweizer, F., Burns, C. R., Madore, B. F., et al. 2008, *AJ*, 136, 1482
- Smith, R. J. 2020, *ARA&A*, 58, 577
- Stanford, S. A., Sargent, A. I., Sanders, D. B., et al. 1990, *ApJ*, 349, 492.
- Stone, R. P. S. & Baldwin, J. A. 1983, *MNRAS*, 204, 347
- Sung, H., Bessell, M. S., Chun, M.-Y., et al. 2017, *ApJS*, 230, 3
- Sung, H., Sana, H., & Bessell, M. S. 2013, *AJ*, 145, 37
- Trancho, G., Bastian, N., Miller, B. W., et al. 2007, *ApJ*, 664, 284
- Trancho, G., Bastian, N., Schweizer, F., et al. 2007, *ApJ*, 658, 993
- van der Hulst, J. M. 1979, *A&A*, 71, 131
- Virtanen, P., Gommers, R., Oliphant, T. E., et al. 2020, *Nature Methods*, 17, 261
- Welty, D. E. 2014, *The Diffuse Interstellar Bands*, 297, 153
- Wenger, M., Ochsenbein, F., Egret, D., et al. 2000, *A&AS*, 143, 9
- Whitmore, B. C., Brogan, C., Chandar, R., et al. 2014, *ApJ*, 795, 156
- Whitmore, B. C., Chandar, R., Schweizer, F., et al. 2010, *AJ*, 140, 75
- Whitmore, B. C. & Schweizer, F. 1995, *AJ*, 109, 960
- Wilson, C. D., Scoville, N., Madden, S. C., et al. 2003, *ApJ*, 599, 1049

Zezas, A., Fabbiano, G., Baldi, A., et al. 2006, ApJS, 166,

211

Zezas, A., Fabbiano, G., Baldi, A., et al. 2007, ApJ, 661,
135

Zhu, M., Seaquist, E. R., & Kuno, N. 2003, ApJ, 588, 243